EPJ Web of Conferences **114**, 01002 (2016)
DOI: 10.1051/epjconf/201611401002

Enhanced pool boiling heat transfer on mini- and micro- structured surfaces

Robert Pastuszko[1,a]

[1]*Kielce University of Technology, Department of Mechanics, Al. Tysiaclecia P.P.7, 25-314 Kielce, Poland*

Abstract. The surfaces used for investigating nucleate pool boiling for four working fluids had mini- and micro-fins of variable configurations, cross-sections and pitches, restrained by perforated foil or mesh cloth with various pore/opening diameters. Unique enhanced structures on these surfaces formed a system of interconnected horizontal and vertical tunnels. Four structured surfaces were proposed, each being a system of subsurface tunnels connected to 10 and 5 mm fins or 1 and 0.5 mm mini-fins. Measurement results for boiling water, ethanol, Fluorinert FC-72 and R-123 from more than 60 samples constituted the database used to verify the proposed theoretical models. These models were based on the results from the visualization studies, including internal visualization allowing observation of bubble nucleation, growth and displacement inside the tunnels, and on the analysis of existing boiling models for mini- and micro-structures.

1 Introduction

Traditional cooling methods based on natural or forced convection used in thermal management of electronic devices and systems are not capable of achieving the required performance in terms of effective heat removal. Harnessing boiling processes occurring on enhanced surfaces with an adequately formed system of subsurface tunnels is a very effective cooling option. The change of phase that accompanies a boiling process provides high heat fluxes at small temperature differences between the heating surface and the saturated fluid, thus increasing the heat transfer coefficient and reducing the size of heat exchanger.

The author of this paper and his collaborators at the Kielce University of Technology have been carrying out in-depth research devoted to determining pool boiling heat transfer coefficients for various working fluids from surface structures with mini- and micro-fins and/or subsurface tunnels and constructing theoretical models [1-7]. At the same time, the research team headed by Dr. M. Piasecka is studying flow boiling heat transfer for FC-72 in rectangular minichannels with enhanced heating surfaces [8,9,10].

This article summarizes the results of the analysis of pool boiling from four types of mini- and micro-structured surfaces.

2 Experimental research

2.1 Investigated surfaces

2.1.1 Tunnel structure (TS) surfaces

The specimens with the tunnel structures (TS) formed a square with sides of length 27 mm (w_f – figure 1).

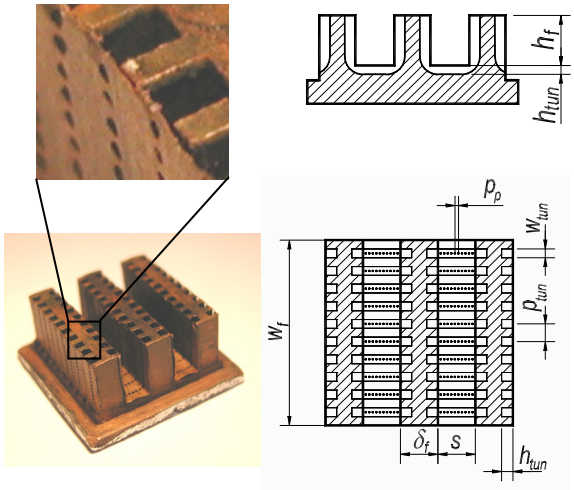

a) b)

Figure 1. TS surfaces investigated: a) views of the sample with 10 mm high fins, b) cross sections [1].

[a] Corresponding author: tmprp@tu.kielce.pl

Three main fins, 5 or 10 mm high (h_f) and 5 mm thick (δ_f), with inter-fin space of 5 mm (s), were modified to create tunnels on the vertical surfaces and in the horizontal inter-fin spaces. Perforated copper foil was sintered to the machined surfaces thereby forming a structure of combined U-shaped tunnels. The following variable parameters were used (figure 1):

- pore diameters: 0.3 – 0.4 – 0.5 mm (d_p),
- pore pitch: 0.6 – 0.8 – 1.0 mm (p_p=2d_p),
- tunnel pitch: 2.0 – 2.25 – 2.5 mm (p_{tun}).

2.1.2 Narrow tunnel structure (NTS) surfaces

The main fins, milled through, formed mini-fins with width corresponding to the thickness of the base fins. In addition, an array of interconnected narrow tunnels was obtained, closed with sintered perforated foil (figure 2). Constant parameters of the main fin geometry were identical to those on TS surfaces. Constant tunnel pitch of 2 mm (p_{tun}) was adopted. Variable parameters of the specimens were as follows:

- pore diameters (d_p): 0.3/0.32 – 0.4 – 0.5 mm,
- narrow tunnel width (w_{tun}): 0.6 – 1.0 – 1.5 mm.

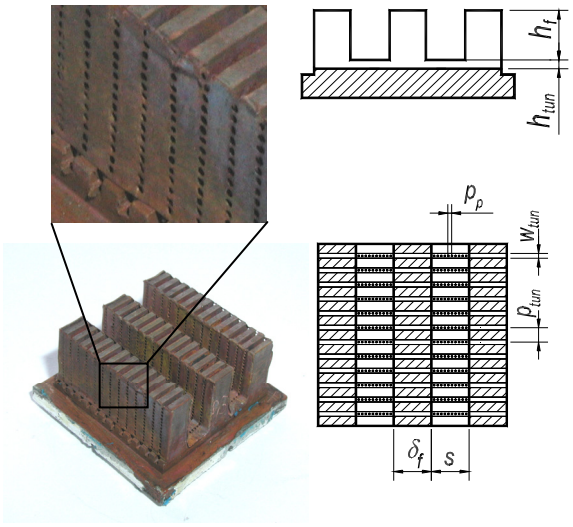

a) b)

Figure 2. NTS surfaces: a) views of the specimen with 5 mm high fins, b) cross sections [1,5].

2.1.3 Mini-fins with porous layer (MF+M/MF+F)

These are structural surfaces formed by sintering the copper wire mesh or perforated foil to the mini-fin tips. The copper specimens, square in shape with a side of 26.5 mm, have 112 mini-fins and form a system of tunnels (figure 3).

The following constant parameters of samples were used:

- mini-fin thickness: 2 mm (δ),
- inter-fin space width: 1.5 mm (s),
- tunnel pitch: 2 mm (p_{tun}).

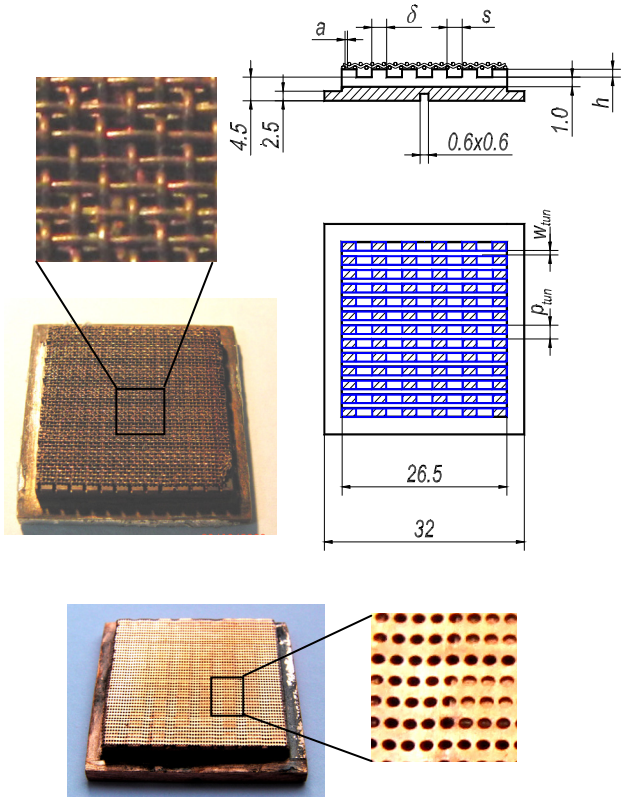

a) b)

Figure 3. MF+M (top) and MF+F (bottom) surfaces: a) views of the specimen, b) cross sections [3,6].

The following parameters were varied (figure 3):

- mesh aperture (a): 0.3 – 0.4 – 0.5 mm
- perforated foil hole diameters (d_p): 0.05 – 0.3 mm
- narrow tunnel width (w_{tun}): 0.6 – 1.0 – 1.5 mm,
- mini-fin height (h): 0.5 – 1.0 mm.

2.2 Experimental set-up

The experimental set-up designed for determining boiling curves and heat transfer coefficients was composed of the four modules and systems (figure 4).

2.3 Working fluids

The following boiling fluids were used:

- distilled water,
- ethyl alcohol,
- refrigerant R-123 – *dichlorotrifluoroethane*,
- fluorinert FC-72 – *perfluorohexane* or *tetradecafluorohexane* (C_6F_{14}).

Table 1 summarizes selected thermodynamic parameters of the liquid and vapour phases at saturation temperature.

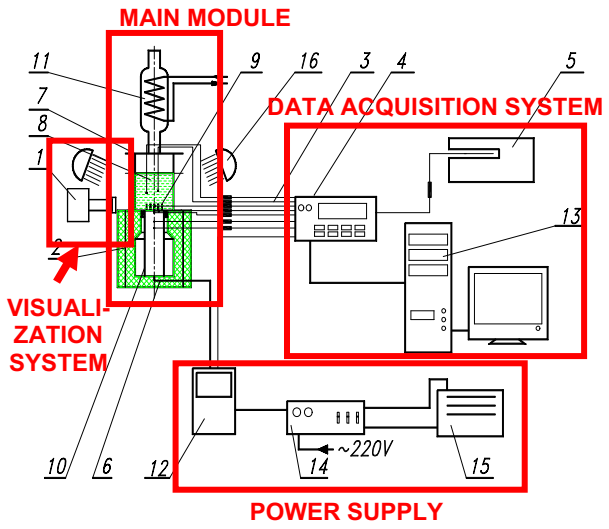

Figure 4. Measuring apparatus: 1 – digital camera, 2 – teflon casing, 3 – compensating leads, 4 – data logger, 5 – dry-well calibrator, 6 – insulation, 7 – glass vessel, 8 – boiling liquid, 9 – investigated sample, 10 – copper bar with cartridge heater, 11 – condenser, 12 – wattmeter, 13 – PC, 14 – power supply and fuses, 15 – autotransformer, 16 – lights.

Table 1. Thermodynamic parameters of the fluids

Saturation parameters (p=101.3 kPa)	Water	Ethanol	FC-72	R-123
T_{sat}, ^{0}C	100	78.3	56.4	27.5
ρ_l, kg/m^3	959	757	1602	1457
ρ_v, kg/m^3	0.597	1.43	13.24	6.39
μ_l, Pa s	$2.82\cdot10^{-4}$	$4.35\cdot10^{-4}$	$4.25\cdot10^{-4}$	$4.06\cdot10^{-4}$
c_l, J/kgK	4220	723	1103	1023
h_{lv}, kJ/kg	2251	963	94.9	170
λ_l, W/mK	0.68	0.169	0.055	0.077
σ_l, N/m	0.0589	0.0177	0.0081	0.015

3 Examples of results

3.1 TS surface – boiling of water

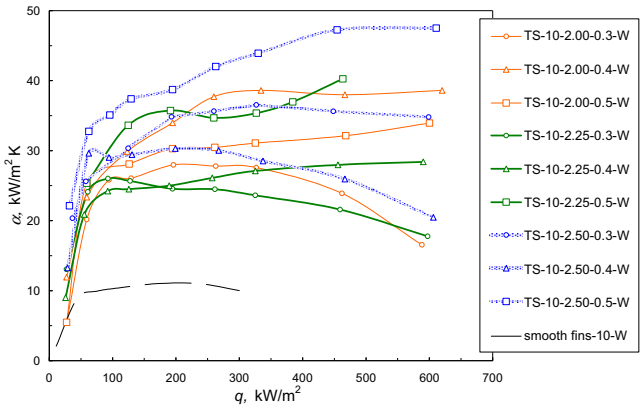

Figure 5. Surfaces with tunnel structure – boiling curves for water, TS surface code: h_f-p_{tun}-d_p; for smooth fins: h_f; W – water [5].

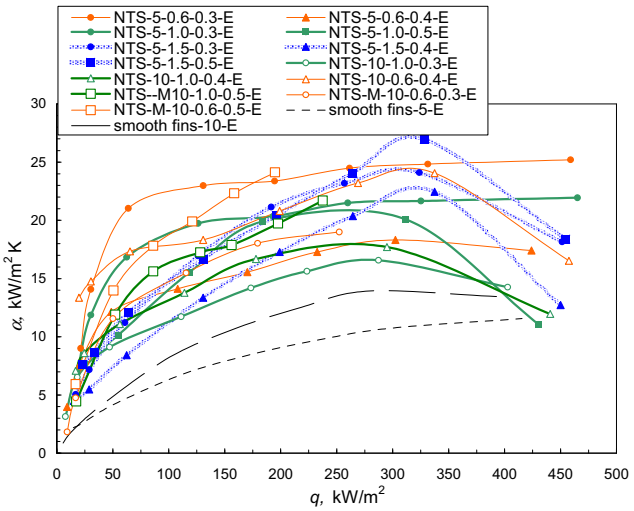

Figure 6. Surfaces with tunnel structure – boiling curves for ethanol, NTS surface code: h_f-p_{tun}-d_p, E – boiling of ethanol

Figure 5 shows the relationships between heat transfer coefficient and heat flux obtained for 10 mm high main fins. The highest heat transfer coefficients, about 47.5 kW/m^{2}K, were noted for the 10 mm fins with tunnels spaced at the highest pitch (2.5 mm) and pores with the largest diameter (0.5 mm).

3.2 NTS surfaces – boiling of ethanol

As for ethanol, NTS surfaces are especially advantageous when the main fins are 5 mm high (figure 6). An increase in heat transfer coefficients for smooth fins (α/α_{sf}) and the NTS-5-0.6-0.3 surface is 3.3 – 2.3 in the range of q = 100 – 300 kW/m^2.

The analysis of ethanol boiling curves for NTS surfaces demonstrates the advantages of coatings with pores 0.3 mm in diameter coupled with the narrowest tunnels (0.6 mm). Two-sided supply in the vertical tunnels compensates evaporation of the ethanol, even when the pores are 0.3 mm in diameter. When 1.5 mm wide tunnels are used, perforated foil with 0.5 mm holes provides the tunnel with suitable supply of fluid, precluding it from evaporating.

3.3 MF+M/MF+F surfaces

Figure 7 compares two types of micro-fin-structured surfaces. The surfaces with micro-fins covered with perforated foil with openings 0.3 mm in diameter can be used only when heat fluxes are low (below 20 kW/m^2). The values of the heat flux coefficient are similar in the range 10 – 100 kW/m^2 for micro-fins covered with foil with openings 0.3 mm in diameter and micro-fins with a mesh when the mesh aperture is 0.5 mm.

Above 40 kW/m^2, plain micro-fins produced the highest heat transfer coefficients, reaching 8 kW/m^{2}K at about 100 kW/m^2. In the range 100 – 150 kW/m^2, the coefficients decreased dramatically. This can be

explained by the dry-out of the inter-micro-fin spaces, a condition that precludes boiling crisis.

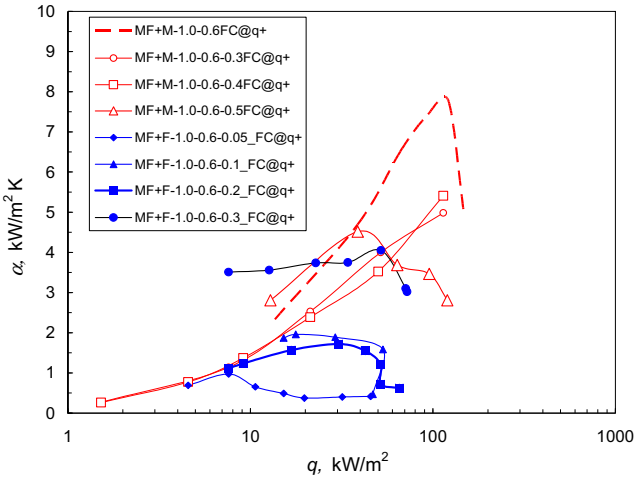

Figure 7. Surfaces with mini-fins with porous layer – boiling curves for FC-72, surface code: h_f-p_{tun}-d_p [3, 6].

4 Examples of boiling visualization

Identification of the phenomena that occur inside the confined space is the necessary condition to meet in order to describe theoretically the boiling process in tunnels, from the initiation to developed nucleate boiling to boiling crisis. To able to analyse nucleate boiling in the complex system of subsurface tunnels, the following data need to be found: the sites of vapour bubble nucleation, growth and departure, the sites of the influx of the fluid into the tunnels, and the sites of determining diameters of the departing bubbles together with their departure frequency.

The visual recording of boiling processes on the surfaces under investigation has been described by the author in several publications [2,4,6]. Examples below illustrate external visualization for the NTS surfaces with 10 mm high main fins.

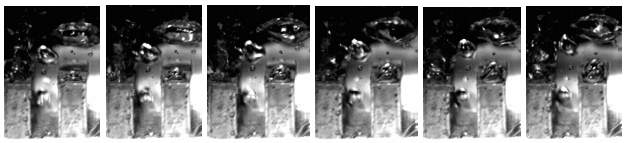

Figure 8. Bubble growth at the vertical tunnel outlet, boiling water: NTS, h_f=10 mm, w_{tun}=1.0 mm, d_p=0.3 mm, ΔT=1.8 K, q=23 kW/m^2, 493 fps (every second frame is shown).

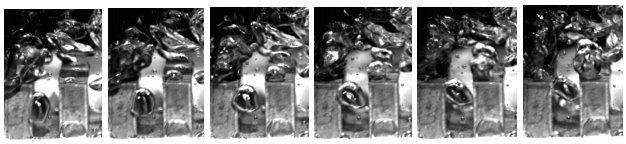

Figure 9. Bubble growth at the vertical tunnel outlet, boiling water, NTS, h_f=10 mm, w_{tun}=1.0 mm, d_p=0.3 mm, ΔT=2.1 K, q=37 kW/m^2, 493 fps (every second frame is shown).

At minor superheats (figure 8), there is a considerable difference in the number of active vertical tunnel outlets in each main fin. The appearing bubbles had spherical shapes; average bubble departure frequency at 1.8 K superheat can be estimated to have reached 16 Hz. The pores in the horizontal tunnels remained inactive.

With increasing superheat (figure 9), a larger number of vertical tunnel outlets become active and some of the departing bubbles are irregular in shape. The frequency of bubble departure increases to about 30 Hz. Marked differences in their diameters are observed.

5 Pool boiling models

Based on the own visualization studies and the existing boiling analytical models, the author proposed the models for boiling from four named above structured surfaces. These models have been thoroughly discussed in [2,4,6].

5.1 Model for TS surface [2]

In the semi-analytical model developed by the author, briefly described below, one of the mechanisms accounted for was the fluid evaporation in the corners of the tunnels, associated with the bubble nucleation cycle. This mechanism was considered together with non-isothermity of the main fin, i.e., assumed one-dimensional temperature distribution along the vertical tunnel walls. Another mechanism taken into account was that of the nucleation, movement and departure of vapour bubbles, different in vertical and horizontal tunnels. This model enables determining diameters of the departing bubbles, their frequency, density of nucleation sites and the overall heat flux for the system of interconnected subsurface tunnels confined with the perforated foil.

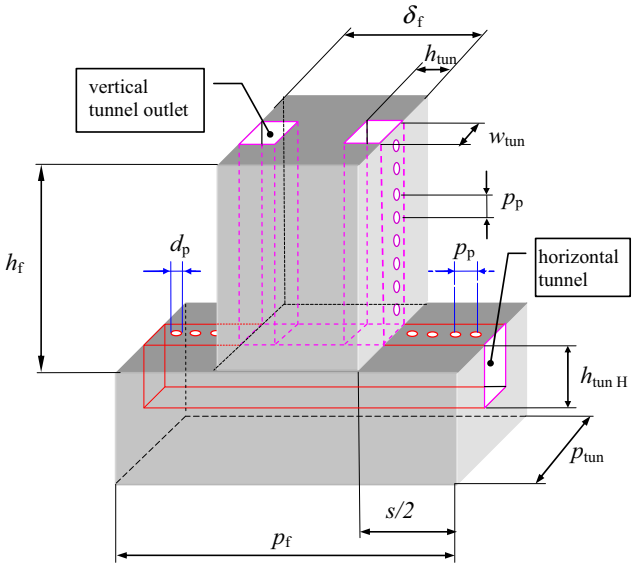

Figure 10. Interconnected vertical and horizontal tunnels of the TS segment in relation to the pitch of main fins and tunnels [2].

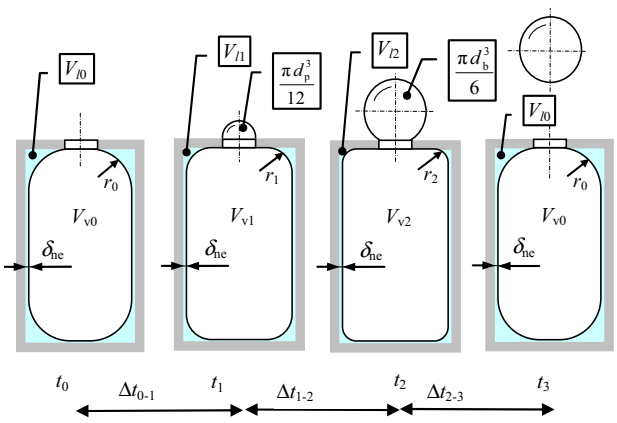

Figure 11. Fluid evaporation in the horizontal tunnel; bubble growth ($\Delta t_{0\text{-}1}$ – waiting period, $\Delta t_{1\text{-}2}$ – growth period, $\Delta t_{2\text{-}3}$ – period of filling with fluid).

5.1.1 Simplifying assumptions

The boiling mechanism in subsurface tunnels (TS – figures 10, 11) is defined by the following major simplifying assumptions:

- the holes in the foil act as elements supplying the surface tunnel structure;
- evaporation occurs from the menisci in the four corners of the tunnels;
- suction and evaporation occur independently for vertical and horizontal tunnels;
- the sites where the bubbles are released, that is, where vapour generated from the menisci in the tunnel corners outflows include: tunnels outlets in vertical tunnels and holes in the foil (pores) in the horizontal tunnels;
- bubble formation cycle in vertical and horizontal tunnels comprises a waiting period ($\Delta t_{0\text{-}1}$), a growth period ($\Delta t_{1\text{-}2}$) and a period of filling with fluid ($\Delta t_{2\text{-}3}$) – figure 11.

5.1.2 Heat flux calculation algorithm for the TS surface

These input data were used:

- Parameters: geometric, of the boiling fluid and the material of the structure: h_{tun}, w_{tun}, p_{tun}, h_f, δ_f, w_f, d_p, p_p, $\rho_{v\,sat}$, ρ_l, σ, λ_v, λ_l, i_{lv}, T_{sat}, λ_{Cu}.
- Literature-based constants: Hamaker's constant, growth period constant $C_{1\text{-}2}$.
- Experimental constants: exponent n in dependence $\alpha \sim \Delta T^{\,n}$

The following algorithm for heat flux determination is proposed:

1. Calculation of vapour density in the horizontal tunnel at the end of the waiting and growth periods.
2. Determination of the volume of fluid in the waiting and growth periods.
3. Calculation of the initial volume of fluid.
4. Calculation of the volume of fluid at the end of growth period according to the relationship.
5. Calculation of the evaporation heat transfer rate.
6. Calculation of the evaporation heat flux in the horizontal tunnel.
7. Determining the waiting and growth periods.
8. Calculation of bubble departure frequency in the horizontal tunnel.
9. Determination of the nucleation site densities in the horizontal tunnel.
10. Determination of the external and overall heat flux for the horizontal tunnel (q_H).
11. Calculation of the volume of fluid for the vertical tunnel according to items 1 – 4, after the introduction of hydraulic diameter.
12. Calculation of evaporation heat transfer rate from the four menisci of the vertical tunnel, using the height of the replacement cross-section.
13. Calculation of fin parameter m_{fm}.
14. Determination of the heat flux in the vertical tunnel ($q_{tun\,V}$).
15. Determination of nucleation site densities for the vertical tunnel (n_{sV}) and the frequency of the bubble departure (f_V).
16. Calculation of the external heat flux for the vertical tunnel (q_{exV}).
17. Calculation of the overall heat flux for the vertical tunnel (q_V).
18. Determination of the overall heat flux for the system of interconnected horizontal and vertical tunnel (q).

Figure 12 compares calculated heat flux and experimental data obtained during the boiling of water.

In the case of flat, homogeneous surfaces with horizontal tunnels, the model is simplified to the calculation of heat flux only according to the procedure for the surfaces with horizontal tunnels – exponent n necessary in the case of the TS complex structures, do not have to be calculated. The calculations were verified against the literature-based measurement data for tunnel structures for the boiling of R-123 and R-11 (figure 13).

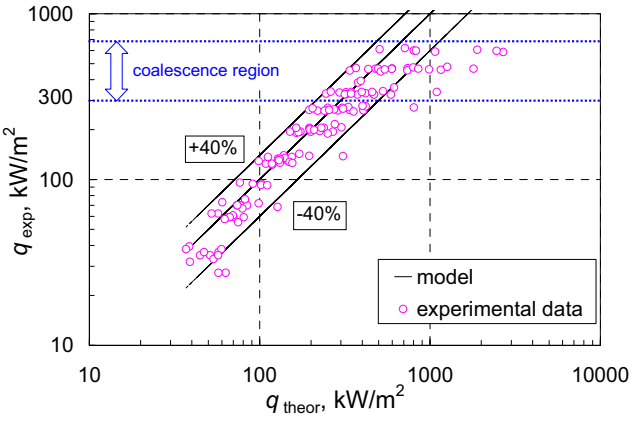

Figure 12. A comparison of experimental and theoretical heat fluxes for the boiling of water [2].

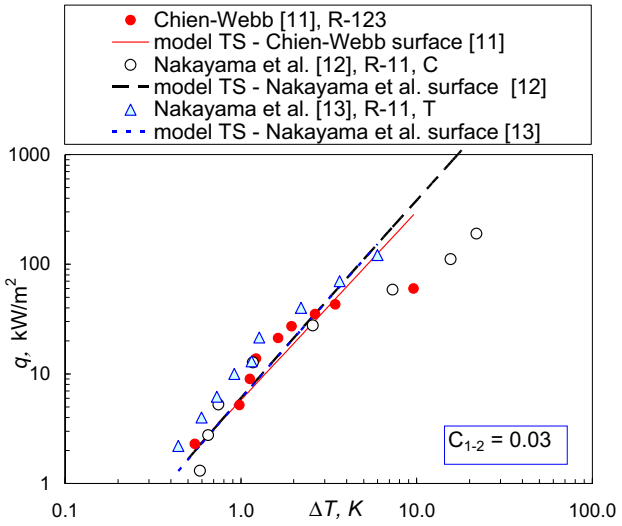

Figure 13. Verification of the model for experimental data from publications [11,12,13].

5.2 NTS surface model

This model, which is a modification of the one presented in [3], treats the area of the vertical tunnel and the area of adjacent horizontal tunnels jointly. One assumption remained – the holes in the foil are made only to supply the tunnels with fluid. Compared with the TS surface model, here the periods of waiting and growth are calculated in a different manner. To provide for the geometry of the structure, the author modified the Mikic and Rohsenow [14] relationship and introduced his own definition of the area of influence.

Additional simplifying assumptions include:

- pores in the horizontal tunnels remain inactive – the bubbles form only at the outlets of vertical tunnel,
- the overall heat flux, calculated jointly for the horizontal and vertical tunnel, comprises the evaporation heat flux inside the interconnected tunnels and the external heat flux associated with bubble departure.

Figure 14 shows the segment of the pitch of the main fins (p_f) and tunnels (p_{tun}) in relation to which the simplified model was formulated.

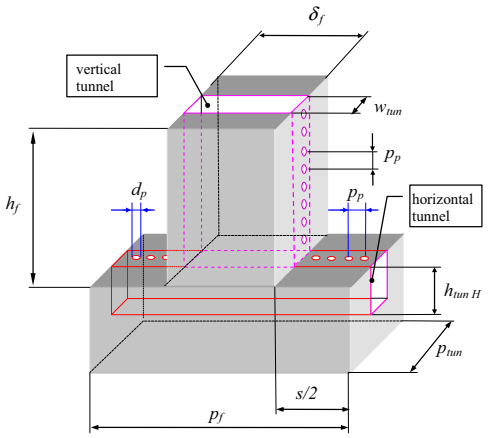

Figure 14. Joined horizontal and vertical tunnels related to the pitch segment volume [4].

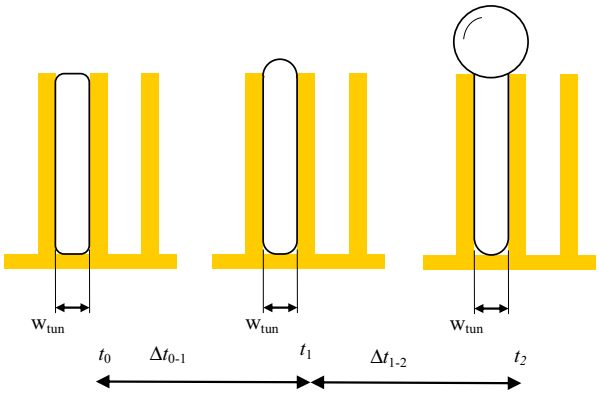

Figure 15. Liquid evaporation stages in the narrow vertical tunnel; bubble growth ($\Delta t_{0\text{-}1}$ – waiting period, $\Delta t_{1\text{-}2}$ – growth period).

The departing bubble diameter for NTS was calculated on the basis of buoyancy force and surface tension balance related to the hydraulic diameter of the vertical tunnel

$$d_{bV} = \left(\frac{6\sigma d_{hV}}{g(\rho_l - \rho_v)} \right)^{1/3} \tag{1}$$

The calculation of the waiting period was based on the modified Mikic and Rohsenow [14] relationship, assuming that this period starts at the moment when the area between the phases at the outlet of the vertical tunnel forms a horizontal plane, and ends when the bubble is formed having a hemispherical shape and the radius equal to the half of the tunnel width, i.e. $R_1=w_{tun}/2$ (figure 15)

$$\Delta t_{0-1} = 0.19 \frac{1}{a_l} \frac{w_{tun}}{Ja} \tag{2}$$

where the Jakob number was defined by: $Ja=c_l \Delta T \rho_l / h_{lv} \rho_v$.

The modified Chien and Webb [15] relationship was used for the calculation of bubble growth period ($\Delta t_{1\text{-}2}$), taken that at the beginning of the growth period the bubble diameter $d_1=w_{tun}$

$$\Delta t_{1-2} = \frac{1}{C_{1\text{-}2}} \left[\frac{7}{\pi} \frac{\rho_l T_{sat}}{h_{lv} \rho_v \Delta T} \frac{(d_{bV} + w_{tun})}{(d_{bV} - w_{tun})} \right]^{1/2} \left(\frac{d_{bV} - w_{tun}}{2} \right) \tag{3}$$

Apart for the fluid supply period, the frequency of bubble departure at the outlet of the vertical tunnel can be calculated as an inverse of the sum of waiting and growth periods:

$$f_V = \frac{1}{\Delta t_{0-1} + \Delta t_{1-2}} \tag{4}$$

The evaporation heat flux in the tunnel is expressed

$$q_{tun} = \rho_v h_{lv} n_{sV} \frac{\pi d_{bV}^3}{6} f_V \tag{5}$$

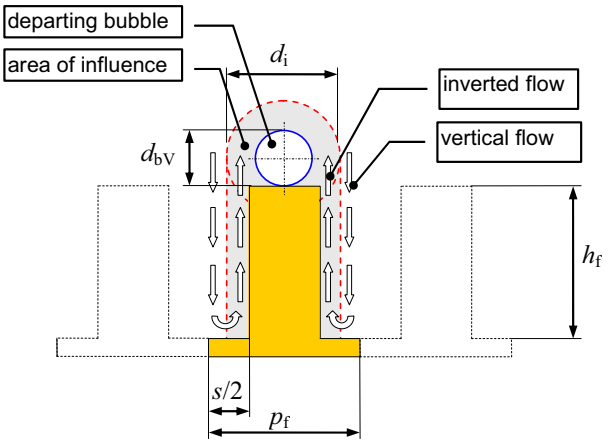

Figure 16. Area of influence for an NTS [4].

With the activity of all vertical tunnel outlets taken to be continuous, the density of nucleation sites remains constant and can be expressed as

$$n_{sV} = \frac{1}{p_{tun}(\delta_f + s)} \tag{6}$$

In relation to the main fin surface, the spatial domain of influence was defined as a surface covering the front of the fin and its lateral planes (figure 16). The dependence for the modified area of influence of the departing bubble has the following form

$$A_i = 2d_{bV}\left(2h_f + d_{bV} + \pi d_{bV}\right) \tag{7}$$

Convective (external) heat flux for defined area of influence is the following

$$q_{ex} = 2n_{sV}A_i\Delta T_{tip}\sqrt{\frac{\lambda_m c_l \rho_l f_V}{\pi}} \tag{8}$$

where ΔT_{tip} is the superheat at the tip of the mini-fin, corresponding to the superheat at the vertical tunnel outlet.

The overall heat flux for the surface with narrow tunnels is expressed by

$$q = q_{tun} + q_{ex} \tag{9}$$

Figure 17 presents a comparison of the experimental and theoretical data.

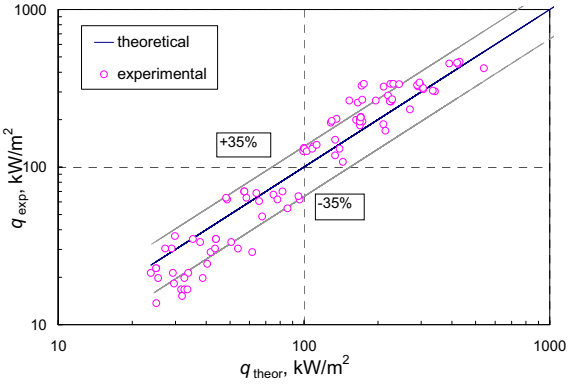

Figure 17. A comparison of experimental and theoretical heat fluxes for the boiling of ethanol [4].

5.3 Simplified model for surfaces MF+M/MF+F [6]

The calculation procedure is similar to that discussed in the previous simplified model (NTS). The diameter of the departing bubble was calculated according to (1). The way for the calculation of the waiting period was changed, assuming after Van Stralen et al. [16] that in pure liquids, the waiting period is related to the growth period by

$$\Delta t_{0-1} = 3\,\Delta t_{1-2} \tag{10}$$

To determine the growth period ($\Delta t_{1\text{-}2}$), d_p was substituted for w_{tun} in relationship (3). The value of $C_{1\text{-}2}$ in this equation was selected through numerical simulation in terms of minimizing errors in the calculation of the frequency of bubble departure and heat flux.

Figure 18 presents the comparison of experimental data for Fluorinert with the values of q calculated from the presented model.

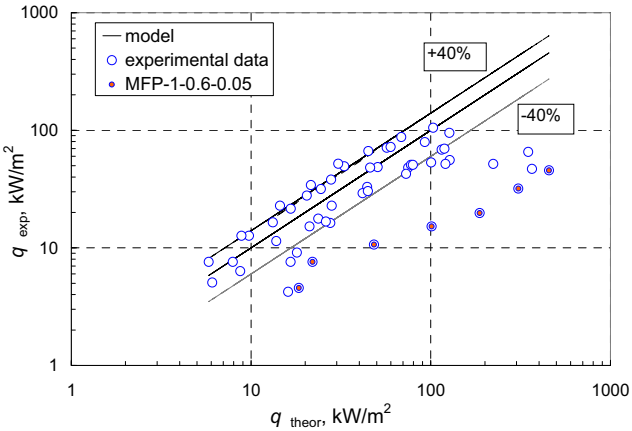

Figure 18. A comparison of experimental and theoretical heat fluxes for MFP surfaces at the boiling of FC-72 at $C_{1\text{-}2}$ = 0.0085 [6].

Conclusions

- Compared with smooth surfaces, the mini and micro structured surfaces allow a substantial heat flux enhancement and up to seven times higher heat transfer coefficients.
- The presented models provide a prediction of heat flux within ±35% – ±40 % error margin for the boiling of water, ethanol and FC-72. Calculations require a selection of two (model for TS) or one experimental constant (NTS and MF+M/MF+F models) in the relationship for the growth period ($C_{1\text{-}2}$).
- These surfaces can be applied to the cooling of elements and systems which generate huge heat fluxes. They can be also used as evaporators of heat pipes or thermosyphons delivering heat to a Stirling engine heater.

References

1. R. Pastuszko, Exp. Thermal Fluid Science **32,** 1564-1577 (2008)
2. R. Pastuszko, M.E. Poniewski, Int. J. Thermal Sciences **47**, 1169-1183 (2008)
3. R. Pastuszko, Int. J. Thermal Sciences **49**, 2289-2298 (2010)
4. R. Pastuszko, Exp. Thermal Fluid Science **38**, 149-164 (2012)
5. R. Pastuszko, EPJ Web of Conferences **45,** 01020 (2013)
6. R. Pastuszko, T.M. Wójcik, Exp. Thermal Fluid Science **63**, 34-44 (2015)
7. R. Pastuszko, M. Piasecka, Journal of Physics: Conference Series **395,** 012137 (2012)
8. M. Piasecka, Annals of Nuclear Energy, **73**, 282-293 (2014).
9. M. Piasecka, Advanced Material Research, **874**, 95-100 (2014)
10. M. Piasecka, Heat Transfer Engineering **35**, 903-912 (2014)
11. L.-H. Chien, R.L. Webb, ASME-HDT **326,** 129-136 (1996)
12. W. Nakayama, T. Daikoku, T. Nakajima, 1982, J. Heat Transfer **104**, 286-291 (1982)
13. W. Nakayama, T. Daikoku, H. Kuwahara, T. Nakajima, Journal of Heat Transfer **102**, 445-450 (1980)
14. B.B.Mikic, W.M.Rohsenow, ASME Journal of Heat Transfer **91,** 245-250 (1969)
15. L.-H. Chien, R.L. Webb, Int. Journal of Heat and Mass Transfer **41**, 2183-2195 (1998)
16. S.J.D.Van Stralen, M.S.Sohal, R.Cole, W.M. Sluyter, Int. J. Heat Mass Transfer **18**, 453-467 (1975)

Nomenclature

a	thermal diffusivity, m^2/s
	mesh aperture, m
A	surface area, m^2
$C_{1\text{-}2}$	growth period constant
c	specific heat at constant pressure, J/kgK
d	diameter, m
f	frequency, Hz
h	height, m
h_{lv}	latent heat of vaporization, J/kg
Ja	Jakob number
MF+F	surface code (mini-fins + perforated foil)
MF+M	surface code (mini-fins + mesh)
NTS	surface code (narrow tunnel structure)
n	exponent in dependence $\alpha \sim \Delta T^n$
n_s	nucleation site density, m^{-2}
p	pitch, m
q	heat flux, W/m^2
R	radius, m
s	gap between fins, m
T	temperature, K
TS	surface code (tunnel structure)
t	time, s
w	width, m

Greek symbols

α	heat transfer coefficient referred to fin base surface, kW/m^2K
ΔT	wall superheat related to fin base surface, K
Δt	period, s
δ	thickness, m
λ	thermal conductivity, W/m K
ρ	density, kg/m^3
σ	surface tension, N/m

Subscripts

0	beginning of the growth period
1	beginning of the waiting period
0-1	waiting
1-2	growth
2-3	intake
b	departing bubble
ex	external
exp	experimental
f	fin
H	horizontal
h	hydraulic
i	influence
l	liquid
m	mean
p	pore
s	smooth
sat	saturation
theor	theoretical
tip	main fin tip
tun	tunnel
V	vertical
v	vapor